Food Bioscience 56 (2023) 103303

Contents lists available at ScienceDirect

Food Bioscience

journal homepage: www.elsevier.com/locate/fbio

# Novel multienzyme cascade for efficient synthesis of D-allulose from inexpensive sucrose

Ruizhi Han [a,*], Wenyu Tu [a], Shuangyu Liu [a], Yu Ji [b], Ulrich Schwaneberg [b,c], Yuanyi Guo [a], Ye Ni [a,**]

[a] Key Laboratory of Industrial Biotechnology, School of Biotechnology, Jiangnan University, Wuxi, 214122, China
[b] Institute of Biotechnology, RWTH Aachen University, Aachen, 52074, Germany
[c] DWI-Leibniz Institute for Interactive Materials, Aachen, 52074, Germany

ARTICLE INFO

*Keywords:*
D-allulose
*In vitro* multienzyme cascade
sucrose
D-allulose 6-phosphate 3-epimerase
ATP-Regeneration system

ABSTRACT

D-Allulose is one of the most common rare sugars with low calorie and is extensively applied in the food, cosmetic, and pharmaceutical fields. Here, a novel *in vitro* multienzyme cascade route (MCAS) was designed to produce D-allulose from sucrose. The MCAS route comprised three modules (sucrose phosphorolysis, phosphorylation–dephosphorylation, and ATP regeneration), including five enzymes (sucrose phosphorylase, fructokinase, D-allulose 6-phosphate 3-epimerase, D-allulose 6-phosphatephosphatase, and polyphosphate kinase). As a rate-limiting enzyme, D-allulose 6-phosphate 3-epimerase from *Pantoea* sp. was semi-rationally engineered, and variant Y143F led to 88.8% yield of D-allulose from 10 mM sucrose using one-pot strategy. ATP consumption was reduced to 5% of the sucrose concentration after introducing ATP-regeneration system. At elevated sucrose concentration of 100 mM by two-step strategy, a D-allulose yield of 70.4% was achieved with a space-time yield of 1.06 g $L^{-1}$·$h^{-1}$. This study provides an efficient and cost-effective approach for producing D-allulose from sucrose.

## 1. Introduction

Rare sugars, representing a group of monosaccharides and sugar alcohols with low abundance in nature (Hayashi et al., 2014; Mijailovic et al., 2021; Mooradian, 2019; Mooradian et al., 2017), are regarded as potential functional sweeteners due to their low calories and various physiological functions (Ahmed et al., 2022; Van Laar et al., 2021). As an important rare sugar, D-allulose (epimer of fructose at C-3 position) is considered an excellent substitute of sucrose because of its 70% sweetness and 0.3% energy (Kimura et al., 2017; Tatsuhiro et al., 2002). Accordingly, D-allulose is extensively applied in baked goods, confectionery, sweet sauces, dairy products, ice cream, desserts, and beverages (Natsume et al., 2021). D-Allulose can also improve the aroma, taste, and color of food by inducing the Maillard reaction (O'Charoen et al., 2015). Moreover, D-Allulose is often used as a metabolic regulator of fattiness and glucose to prevent obesity and type 2 diabetes mellitus (Hossain et al., 2015) due to its strong anti-hyperlipidemic and anti-hyperglycemic effects (Chung et al., 2012; Han et al., 2020; Hayashi et al., 2010; Iida et al., 2008; Natsume et al., 2021; Gou et al., 2021; Jiang & Fang, 2016). Given its inhibitory effect on reactive oxygen species (Mooradian et al., 2019; Suna et al., 2007) and cancer cell proliferation, D-allulose is also often used as an adjuvant for treating neurological tissue degeneration and atherosclerosis (Murao et al., 2007; Takata et al., 2005).

D-Allulose is scarce in nature and exists only in extremely small quantities of plants (Andreana et al., 2002). Thus, most D-allulose is synthesized by chemical and biological methods. Generally, the chemical synthesis of ketohexose primarily depends on selective aldol reactions synthesis, catalytic hydrogenation, addition reaction, and Ferrier rearrangement (Northrup & MacMillan, 2004). Consequently, the following two processes contribute to the chemical synthesis of D-allulose: (i) one-step isomerization of D-glucose or D-fructose using molybdenum, and (ii) multistep synthesis of D-allulose using base. However, these chemical methods for D-allulose synthesis have low potential for industrialization due to their poor economy, environment unfriendliness, and low availability. Biotransformation from D-fructose using D-tagatose-3 epimerase is a potential approach to the production of

* Corresponding author.
** Corresponding author.
*E-mail addresses:* hanrz@jiangnan.edu.cn (R. Han), yni@jiangnan.edu.cn (Y. Ni).

https://doi.org/10.1016/j.fbio.2023.103303
Received 17 September 2023; Received in revised form 16 October 2023; Accepted 24 October 2023
Available online 27 October 2023

**List of abbreviations**

| | |
|---|---|
| (MCAS) | multienzyme cascade for D-allulose synthesis from sucrose |
| (SP) | sucrose phosphorylase |
| (FRK) | fructokinase |
| (A6PE) | D-allulose 6-phosphate 3-epimerase |
| (A6PP) | D-allulose 6-phosphatephosphatase |
| (PPK) | polyphosphate kinase |
| (DNS) | dinitrosalicylic acid |
| (G1P) | glucose-1-phosphate |
| (F6P) | fructose-6-phosphate |
| (A6P) | D-allulose-6-phosphate |

D-allulose, however it suffers less than 50% of conversion due to inevitable reversible reaction (Itoh et al., 1994; Wang et al., 2020). For instance, D-tagatose-3 epimerase from *Rhodopirellula baltica* obtained by gene mining and protein engineering could produce 28.6% yield of D-allulose (Mao et al., 2020). One two-enzyme strategy comprising D-allulose-3 epimerase and *exo*-inulinase were performed for D-allulose synthesis from inulin in Jerusalem artichoke (JA), leading to a 13.4% D-allulose yield from JA powder (Zhu et al., 2020). Subsequently, after combining a NGTag/NGCatcher/CsgA system with the two-enzyme (D-allulose-3 epimerase and *exo/endo*-inulinase) strategy, a final productivity of 0.25 g L·min$^{-1}$ from 100 g/L inulin was achieved (Chen et al., 2023). Although the yield increased to 64.5% after adding borate, a mass of byproducts (e.g., D-allulose-borate complex) were also generated (Kim et al., 2008; Lim et al., 2009). The multienzyme cascade pathway was developed to break the thermodynamic limitation, yielding up to 79.2% of D-allulose from 50 g L$^{-1}$ soluble starch with a space-time yield of 0.37 g L$^{-1}$·h$^{-1}$ (Li et al., 2021). However, this route was inefficient since lots of enzymes were involved and many by-products could be generated. Therefore, an efficient and low-cost approach for the production of D-allulose is urgently necessary.

Sucrose is a low cost and abundant disaccharide around the world, but its excessive intake increases the risk of many potential diseases (e.g., obesity and hyperglycemia) (Qi & Tester, 2020). Sucrose is often used as a raw material for the synthesis of high-value products, such as cellobiose (Kitaoka et al., 1992), α-D-glucoside (Goedl et al., 2009), rhamnolipid (Bahia et al., 2018), and kojibiose (Wang et al., 2018). Herein, a novel multienzyme cascade route for synthesizing D-allulose from sucrose (denoted as the MCAS route) was designed. It comprised three modules (sucrose phosphorolysis, phosphorylation–dephosphorylation, and ATP regeneration) and five enzymes (sucrose phosphorylase (SP), fructokinase (FRK), D-allulose-6-phosphate 3-epimerase (A6PE), D-allulose 6-phosphate phosphatase (A6PP), and polyphosphate kinase (PPK)). After route optimization and engineering of the rate-limiting enzyme A6PE, final D-allulose yield of 88.8% was achieved from 10 mM sucrose. Introducing ATP-regeneration system further reduced the cost and enhanced the sustainability of this cascade process. Finally, elevated concentrations of sucrose were also attempted and optimized.

## 2. Materials and methods

### 2.1. Plasmids, strains and chemicals

All strains and plasmids used in this study are listed in Table S1. *Escherichia coli* BL21 (DE3) was purchased from Takara (Dalian, China) and used as the host for recombinant enzyme expression. Plasmids pET-28a (+) served as vectors for expression. Genes encoding sucrose phosphorylase from *Bifidobacterium adolescentis* (*Ba*SP, GeneBank ID: WP_011742626.1), fructokinase from *Clostridium acetobutylicum* (*Ca*FRK, GeneBank ID : KHD36265.1), D-allulose 6-phosphate 3-epimerase from *Pantoea* sp (*Psp*A6PE, GeneBank ID : WP_039379501.1), D-allulose 6-phosphate phosphatase from *Clostridium thermocellum* (*Ct*A6PP, GeneBank ID : WP_003512401.1), and polyphosphate kinase from *Deinococcus radiodurans* (*Dr*PPK, GeneBank ID : WP_010886780.1) were synthesized by Exsyn Bio Co., Ltd. (Shanghai, China). The standards of D-allulose, fructose and sucrose were purchased from Yuanye Bio-Technology Co., Ltd (Shanghai, China). ATP and ADP were procured from Bidepharm (Shanghai, China). Other chemicals were purchased from Sangon Biotech (Shanghai, China).

### 2.2. Cloning and expression of enzymes

Gene fragments (*Ba*SP, *Ca*FRK, *Ct*A6PP, *Psp*A6PE, and *Dr*PPK) were individually cloned into plasmid pET-28a(+) with the restriction endonucleases *Bam* HI and *Xho* I. The recombinant plasmids were then transformed into the host *E. coli* BL21 (DE3) for expression. Then, these recombinant *E. coli* strains were inoculated in Luria–Bertani (LB) media containing 50 μg mL$^{-1}$ kanamycin at 37 °C with shaking at 220 rpm overnight. Subsequently, the overnight incubated cultures were transferred to new LB media at an inoculation of 1% (v/v). After induction with 0.2 mM isopropyl-β-D-thiogalactopyranoside (IPTG) at an optical density at 600 nm of 0.6–0.8, the culture was further incubated on a rotary shaker (220 rpm) at 16 °C for 20 h. Cells were then harvested by centrifugation at 8000×*g* and 4 °C for 5 min.

### 2.3. Purification of enzymes

The collected cells were resuspended in 50 mM Tris-HCl buffer (pH 8.0) and sonicated on ice for 10 min (power = 300 W). Then, the disrupted solution was centrifuged at 4 °C, 8000×*g* for 30 min, and the supernatant was passed through a 0.45 μm filter membrane. Crude enzymes were purified using a Ni-NTA affinity column (Qiagen, Chatsworth, CA, USA). The purity of each enzyme was determined by sodium dodecyl sulfate polyacrylamide gel electrophoresis (SDS-PAGE).

### 2.4. Enzymatic activity analysis

SP activity was measured by dinitrosalicylic acid (DNS) colorimetry. The reaction mixture (1.5 mL) containing 400 μL of sucrose (1.48 M), 1090 μL of PBS buffer (50 mM, pH 7.0), and 10 μL of enzyme was accurately incubated at 50 °C for 10 min. Then, 3 mL of DNS solution was added and incubated in boiling water for 10 min. After cooling to room temperature, the mixture was adjusted to 10 mL using deionized water, and the absorbance value at 540 nm was detected. One unit of SP was defined as the amount of enzyme required to hydrolyze sucrose to 1 μmol fructose by free enzyme per minute.

FRK activity was determined as follows. A mixture containing 50 mM Tris-HCl (pH 8.0), 10 mM fructose, 1 mM $MgCl_2$. and 10 mM ATP was incubated at 40 °C for 10 min. The reaction was terminated in boiling water for 10 min. The concentration of fructose was assayed by HPLC. One unit of FRK was defined as the amount of enzyme that consumed 1 μmol fructose per minute.

A6PE activity was measured by coupling A6PP as follows. A reaction mixture containing 50 mM Tris-HCl (pH 8.0), 2 mM F6P, 1 mM $CoCl_2$, 0.2 U·mL$^{-1}$ A6PP, and 0.01 mg mL$^{-1}$ A6PE was incubated at 40 °C for 20 min. The reaction was stopped with boiling water for 10 min, and the released inorganic phosphate was measured by mild pH phosphate assay[26]. One unit of enzyme activity was defined as the amount of enzyme that released 1 μmol of phosphate per minute.

A6PP activity was measured through a coupled enzyme reaction with A6PE. The reaction was performed at 40 °C for 20 min in 50 mM Tris-HCl (pH 8.0) including 2 mM F6P, 1 mM $CoCl_2$, 1 mg mL$^{-1}$ A6PP, and 1.5 U·mL$^{-1}$ A6PE. One unit of A6PP was defined as the amount of enzyme required to produce 1 μmol D-allulose 6-phosphate per minute.

### 2.5. Optimization of reaction Module I

The reaction of Module I was performed in a 5-mL tube containing 2 mL of mixture, which comprised 10 mM D-fructose, 10 mM ATP, 50 mM phosphate buffer (pH 7.0), and three enzymes (*Ca*FRK, *Psp*A6PE, and *Ct*A6PP). The initial reaction temperature and pH were 50 °C and 7.0, respectively. After incubation for 48 h, the reaction mixture was terminated with boiling water for 10 min, and the concentration of D-allulose was measured by HPLC.

HPLC was performed using an Agilent 1260 HPLC system equipped with a CarboPac $Ca^{2+}$ column (300 mm × 8 mm) and a refractive index detector. Mobile phase (pure water) was used for elution at 80 °C at a flow rate of 0.9 mL $min^{-1}$. A 10 μL sample was injected into the analytical HPLC by using an automatic sampler.

The reaction conditions (temperature, pH, enzyme ratio, metal ions, and ATP concentration) of Module I were optimized as follows. Based on the initial conditions, the influence of reaction temperature (35, 40, 45, 50, 55, and 60 °C) and pH (5.0, 5.5, 6.0, 6.5, 7.0, 7.5, 8.0, 8.5, 9.0, and 9.5) on D-allulose biosynthesis was investigated. Based on the optimum reaction temperature and pH, the effect of loading enzymes ratio (*Ca*FRK–*Psp*A6PE–*Ct*A6PP) on the biosynthesis of D-allulose was also investigated. To further improve the yield of D-allulose, ATP concentrations (0, 2, 5, 10, and 15 mM) and metal ions ($Mg^{2+}$, $Mn^{2+}$, $Co^{2+}$, $Ca^{2+}$ and $Zn^{2+}$) were optimized.

### 2.6. Homologous modeling of PspA6PE and molecular docking

The structure model of *Psp*A6PE was built using Discovery Studio 4.5 software package by using the crystallographic structure of A6PE from *E. coli* (PDB ID: 3CT7, 58.5% sequence identity with *Psp*A6PE) as template. Molecular-docking simulations with fructose-6-phosphate (F6P) as the ligand were performed using the CDOCKER module under a default setting within the active site defined by the Binding-Site module.

### 2.7. Site-directed saturation mutagenesis of PspA6PE

Site-directed mutagenesis of *Psp*A6PE was performed using whole-plasmid PCR with pET28a-*Psp*A6PE as template. The primers for alanine scanning and site-directed saturation mutagenesis were listed in Tables S2 and S3. The PCR program was as follows: 94 °C (5 min); 30 cycles of 98 °C (10 s), 55 °C (30 s) and 68 °C (30 s); 68 °C (10 min) and final hold at 16 °C. After digestion with *Dpn* I at 37 °C for 1 h, the PCR mixture was transformed into *E. coli* BL21 (DE3) and confirmed by sequencing. All confirmed variants were expressed and purified with the same procedure as mentioned above for the wild-type *Psp*A6PE.

A high-throughput screening method was established using molybdenum blue method (Saheki et al., 1985). In a typical procedure, a 96-well plate was used to culture the bacteria. After the cells were collected, the solution (50 mM Tris-HCl, 750 mg $L^{-1}$ lysozyme, and 10 mg $L^{-1}$ DNase) was added to each well, and the cells were lysed at 37 °C for 1 h. The supernatant obtained after centrifugation was the crude enzyme solution. Then, the enzyme-activity method described in Section 2.4 was used for screening.

### 2.8. Kinetic analysis of PspA6PE and its variants

The activities of *Psp*A6PE and its variants were assayed with F6P substrate in different concentrations of 0.5–40 mM in Tris-HCl buffer (50 mM, pH 8.0) at 40 °C. The values of $K_m$ and $V_{max}$ were calculated by the Michaelis−Menten equation using Origin pro 8.6 software. The $k_{cat}$ and $k_{cat}/K_m$ were also calculated for WT and variants.

### 2.9. Construction of Module II for ATP-regeneration

To reduce the consumption of ATP, an ATP-regeneration system was constructed by introducing *Dr*PPK. The initial reaction mixture contained 50 mM Tris HCl buffer (pH 8.0), 10 mM D-fructose, 2 mM ATP, 2 mM sodium hexametaphosphate, 2 mM $CoCl_2$, 0.56 U·$mL^{-1}$ (0.4 μM) *Ca*FRK, 0.38 U·$mL^{-1}$ (0.8 μM) *Psp*A6PE, 0.001 U·$mL^{-1}$ (0.4 μM) *Ct*A6PP, and 0.02 mg $mL^{-1}$ (0.5 μM) *Dr*PPK. Subsequently, the effects of metal ions, ATP, and sodium hexametaphosphate concentrations were investigated.

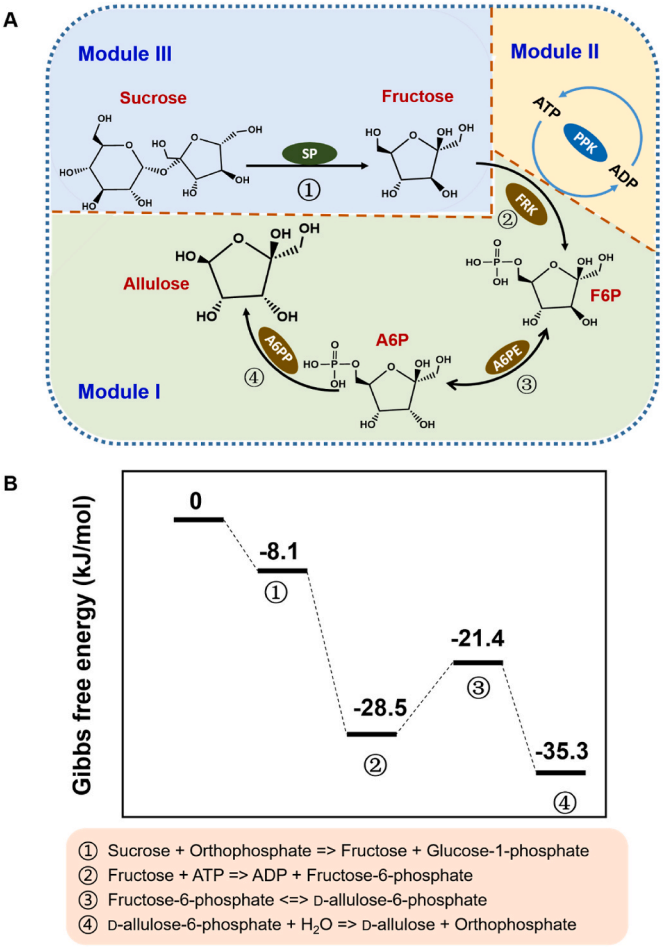


**Fig. 1. (A)** Schematic of D-allulose synthesis from sucrose via an *in vitro* multienzyme cascade biosystem (MCAS) developed in this study. The whole MCAS comprises three modules and five enzymes: Module I (FRK, A6PE, and A6PP), Module II (PPK), and Module III (SP). **(B)** Standard Gibbs free energy change for the overall reaction. The change in Gibbs free energy is freely available at: http://equilibrator.weizmann.ac.il.

### 2.10. Construction of Module III for sucrose phosphorylation

A reaction system was established with sucrose as substrate, including 10 mM PBS (pH 8.0), 10 mM sucrose, 0.5 mM ATP, 2 mM sodium hexametaphosphate, 4 mM $MgCl_2$, 8.78 U·$mL^{-1}$ (0.15 μM) *Ba*SP, 0.56 U·$mL^{-1}$ (0.4 μM) *Ca*FRK, 0.38 U·$mL^{-1}$ (0.8 μM) *Psp*A6PE, 0.001 U·$mL^{-1}$ (0.4 μM) *Ct*A6PP, and 0.02 mg $mL^{-1}$ (0.5 μM) *Dr*PPK.

### 2.11. Biosynthesis of D-allulose through MCAS route from an elevated concentration of sucrose

An elevated concentration of sucrose (20, 50, and 100 mM) was attempted in the MCAS route for D-allulose production. The reaction was performed in a 5 mL tube containing 2 mL of mixture, and the initial reaction conditions were as follow: 10 mM PBS (pH 8.0), 4 mM $MgCl_2$, 0.5 mM ATP, 2 mM sodium hexametaphosphate, *Ba*SP (8.78 U·$mL^{-1}$, 0.15 μM), *Ca*FRK (0.56 U·$mL^{-1}$, 0.4 μM), *Psp*A6PE (0.38 U·$mL^{-1}$, 0.8

μM), *Ct*A6PP (0.001 U·mL$^{-1}$, 0.4 μM), and *Dr*PPK (0.02 mg mL$^{-1}$, 0.5 μM). Incubation was conducted at 40 °C for 24 h. The enzymes dosage and co-substrates were optimized, and the concentration of D-allulose was determined by HPLC.

## 3. Results and discussion

### 3.1. Design of MCAS route for D-allulose synthesis from sucrose

A novel *in vitro* multienzyme cascade (MCAS) route was designed for the biosynthesis of D-allulose from sucrose. It comprises three modules involving five enzymes (SP, FRK, A6PE, A6PP, and PPK) (Fig. 1A). (1) Module I (phosphorylation–dephosphorylation) is a cascade synthesis of D-allulose from D-fructose using three enzymes (FRK, A6PE, and A6PP). In this module, the phosphorylation of fructose to fructose-6-phosphate (F6P) is catalyzed by FRK in the presence of ATP. Subsequently, F6P is epimerized to D-allulose-6-phosphate (A6P) by A6PE and then further dephosphorylated to generate D-allulose by A6PP. (2) Module II is an ATP-regeneration system. In this module, ATP synthesis from ADP is catalyzed by PPK, which is coupled with the phosphorylation of fructose catalyzed by FRK (from ATP to ADP). (3) Module III (sucrose phosphorolysis) is the synthesis of D-fructose from sucrose by phosphorolysis of SP.

Generally, the Gibbs free energy change (ΔG) can reflect the system's thermodynamics stability (Ji et al., 2023). According to the second law of thermodynamics, the system becomes more stable with the lower Gibbs free energy (Dobson, 2004). Therefore, herein the standard Gibbs free energy was calculated to identify the thermodynamic feasibility of MCAS route (apart from Module II). As shown in Fig. 1B, the overall $\Delta G'^{0}$ of sucrose to D-allulose is −35.3 kJ mol$^{-1}$, indicating that generating D-allulose from sucrose by this cascade route is thermodynamically favorable.

To further explore the proof-of-concept experiment of this process, a 2 mL reaction mixture comprising above five enzymes (Table S4) was incubated at 50 °C for 48 h, and the products were determined by HPLC. As shown in Fig. S1, compared with the controls, a new peak at an approximate retention time of 21 min was detected in the reaction mixture. This product is consistent with the D-allulose standard, indicating the feasibility of the synthesis of D-allulose from sucrose through MCAS route.

In this MCAS route, the synthesis of high-value D-allulose from sucrose was achieved with reduced cost after introducing ATP-regeneration system (Module II). Compared with the traditional one-step epimerization of D-fructose to D-allulose using D-tagatose 3-epimerase (Wang et al., 2020), the MCAS route theoretically broke the thermodynamic equilibrium due to the irreversibility of the last step (conversion of D-allulose-6-phosphate to D-allulose catalyzed by A6PP). Moreover, the substrate cost was decreased by replacing D-fructose with sucrose. According to the reported multi-enzymes cascade strategy (Li et al., 2021), numerous enzymes were involved (e.g., α-glucan phosphorylase, phosphoglucomutase, phosphoglucose isomerase, D-allulose 6-phosphate 3-epimerase, and D-allulose 6-phosphate phosphatase, isoamylase, 4-α-glucanotransferase, polyphosphate glucokinase, and glucose isomerase), and many by-products could be generated (e.g., glucose, fructose, glucose-1-phosphate (G1P), glucose-6-phosphate (G6P), fructose-6-phosphate (F6P), and D-allulose-6-phosphate (A6P)) (Fig. S2). In this MCAS route, the cascade biosynthesis of D-allulose were simplified with less enzymes and intermediate products (Fig. S2). To further enhance the yield of D-allulose via MCAS route, Modules (I, II, and III) were optimized as follows.

### 3.2. Optimization of Module I (D-fructose to D-allulose)

#### 3.2.1. Identification and gene mining of the rate-limiting enzyme

In Module I, FRK from *C. acetobutylicum* (*Ca*FRK), A6PE from *T. thermosaccharolyticum* (*Tt*A6PE), and A6PP from *C. thermocellum* (*Ct*A6PP) were initially selected due to their performance properties of activity and thermostability (Li et al., 2021; Xu et al., 2020). However, a low yield of D-allulose (3.1%) was obtained from D-fructose through the cascade reaction by using these three enzymes. To identify the rate-limiting enzyme of this module, different loading amounts of each enzyme were investigated. As shown in Fig. 2A, the yield of D-allulose increased from 3.1% to 6.2% with 10-fold *Tt*A6PE dosage compared with the initial attempt, whereas D-allulose yield was not significantly changed when using 10-fold dosage of *Ca*FRK and *Ct*A6PP, indicating the rate-limiting enzyme of A6PE in module I.

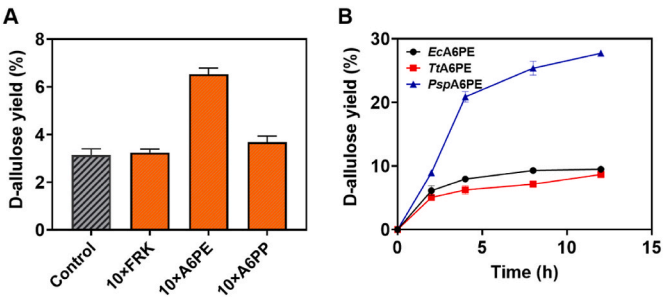


**Fig. 2.** Identification and mining of the rate-limiting enzyme **(A)** Identification of the rate-limiting step in Module I. The initial reaction mixture (2 mL) of the control group including 50 mM PBS buffer (pH 7.0), 10 mM fructose, 0.4 μM purified *Ca*FRK, 0.4 μM purified *Tt*A6PE, and 0.4 μM purified *Ct*A6PP was carried out at 50 °C for 12 h. 10 × FRK, 10 × A6PE, and 10 × A6PP mean that the concentrations of FRK, A6PE and A6PP enzymes were increased to 10-fold of their initial concentrations. **(B)** Production of D-allulose from fructose using one-pot strategy by using *Ec*A6PE, *Tt*A6PE, and *Psp*A6PE. Reaction mixture of 2 mL including 10 mM D-fructose, 10 mM ATP, 50 mM phosphate buffer (pH 7.0), 0.4 μM purified *Ca*FRK and 0.4 μM purified *Ct*A6PP, and 4 μM purified A6PE enzyme (*Ec*A6PE, *Tt*A6PE or *Psp*A6PE) was performed at 50 °C. Values are presented as the mean ± SD from triplicate measurements.

Subsequently, gene mining of A6PE was performed with BLAST (https://www.ncbi.nlm.nih.gov/) using *Tt*A6PE as a probe. A6PEs from *Pantoea* sp. BRM17 (*Psp*A6PE) and *E. coli* K-12 (*Ec*A6PE) were selected as candidate enzymes with >55% sequence identity to *Tt*A6PE. Then, the cascade reaction was performed using above A6PEs (e.g., *Ec*A6PE, *Tt*A6PE, and *Psp*A6PE) in a 2-mL reaction mixture, respectively. As shown in Fig. 2B, the yield of D-allulose increased to 27.7% at 12 h using *Psp*A6PE, which was 3-fold of that using *Ec*A6PE and *Tt*A6PE. Therefore, *Psp*A6PE was selected for further investigations.

#### 3.2.2. Optimization of reaction conditions

The reaction conditions of Module I were optimized to further improve the yield of D-allulose. As shown in Fig. 3A, the highest yield of D-allulose (18.4% at 24 h) was obtained at 40 °C. Based on the optimum temperature (40 °C), the effects of reaction pH (5.0–9.5) on the yields of D-allulose were also investigated. Overall, the yields of D-allulose were higher within the alkaline range than acidic condition. In particular, D-allulose showed higher yields in Tris-HCl buffer (pH 7.5–9.0) than in other buffers, and the highest yield of 23.2% was reached at pH 8.0 (Fig. 3B).

Multienzymes generally exert a complicated performance in cascade reactions, requiring different amount of each enzyme. In the present study, the enzyme-loading ratio (*Ca*FRK–*Psp*A6PE–*Ct*A6PP) was also optimized. As shown in Fig. 3C, the yield of D-allulose increased to 29.5% at an enzyme ratio of 1:2:1 (including 0.4 μM *Ca*FRK, 0.8 μM *Psp*A6PE, and 0.4 μM *Ct*A6PP). As the rate-limiting enzyme, increased *Psp*A6PE loading was beneficial to the yield of D-allulose. With an increased multienzyme ratio (*Ca*FRK–*Psp*A6PE–*Ct*A6PP) of 1:3:1, the yield of D-allulose (30.4%) was slightly higher than that at 1:2:1. Considering the cost of enzymes, the optimum ratio of multienzymes (*Ca*FRK–*Psp*A6PE–*Ct*A6PP) was determined to be 1:2:1.

*Ca*FRK is an ATP-dependent enzyme, and the effect of various

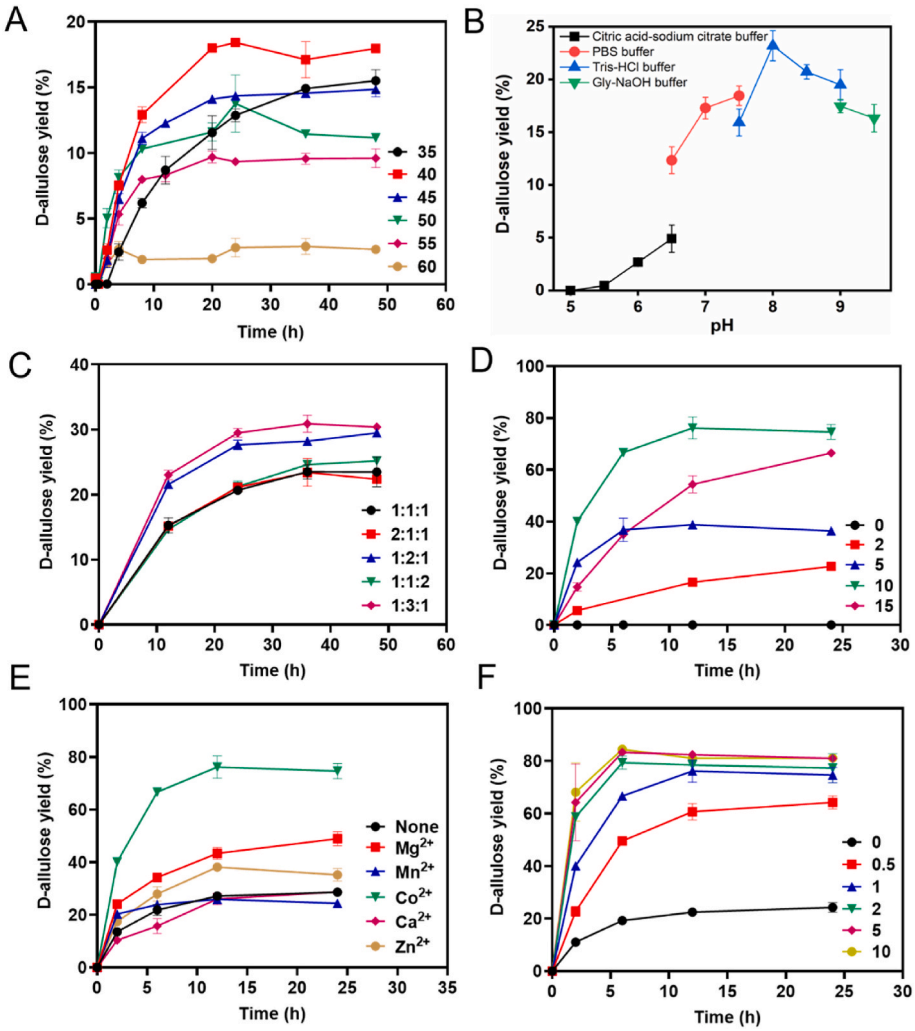


**Fig. 3.** Optimization of reaction conditions for D-allulose production in terms of temperature **(A)**, pH **(B)**, enzyme ratio **(C)**, ATP concentrations **(D)**, metal ions **(E)**, and $Co^{2+}$ concentrations **(F)**. Values were presented as the mean ± SD from triplicate measurements. The initial conditions were 10 mM D-fructose, 10 mM ATP, 50 mM PBS buffer (pH 7.0), 0.4 μM purified *Ca*FRK, 0.4 μM purified *Ct*A6PP, and 0.4 μM purified *Psp*A6PE.

concentrations of ATP was also investigated. As shown in Fig. 3D, the yield of D-allulose reached the highest (76%) at 24 h with an ATP concentration of 10 mM, and a significantly decreased D-allulose was observed with ATP concentrations less than 10 mM. However, with increased ATP concentration to 15 mM, the yield of D-allulose also slightly decreased compared with that at 10 mM, which may be attributed to the inhibitory effect of excess ATP.

Afterwards, the effects of metal cations in module I were investigated. Various metal ions (1 mM of $Mn^{2+}$, $Ca^{2+}$, $Co^{2+}$, $Mg^{2+}$, and $Zn^{2+}$) were added to the cascade reaction system. Compared with the control (without metal ions), addition of $Co^{2+}$, $Mg^{2+}$, and $Zn^{2+}$ resulted in increased D-allulose yield by 3.2-, 1.9-, and 1.3-fold, whereas $Mn^{2+}$ and $Ca^{2+}$ slightly inhibited the cascade effect (Fig. 3E). Subsequently, the concentration of $Co^{2+}$ was optimized. As shown in Fig. 3F, with increased $Co^{2+}$ concentration from 0 to 2 mM, the yield of D-allulose increased from 20% to 79% at 6 h, and nearly kept constant with prolonged time (6–24 h). With high concentrations of $Co^{2+}$ (e.g., 5 and 10 mM), the yields of D-allulose were similar to that with 2 mM $Co^{2+}$. Consequently, to avoid excess heavy-metal ion, 2 mM $Co^{2+}$ was selected for further investigation.

Therefore, the optimum conditions for the synthesis of D-allulose from 10 mM fructose (Module I) were determined as follows: 2 mL of reaction mixture containing 50 mM Tris-HCl buffer (pH 8.0), 10 mM ATP, 2 mM $CoCl_2$, 0.4 μM (0.56 $U{\cdot}mL^{-1}$ equivalent) *Ca*FRK, 0.8 μM (0.38 $U{\cdot}mL^{-1}$ equivalent) *Psp*A6PE, and 0.4 μM (0.001 $U{\cdot}mL^{-1}$ equivalent) *Ct*A6PP, incubated at 40 °C for 6 h. Under above condition, 79.3% of yield of D-allulose was obtained, which was 4-fold higher than that under the initial conditions.

### 3.3. Semi-rational engineering of PspA6PE and mechanism analysis

To further improve the yield of D-allulose, the rate-limiting enzyme *Psp*A6PE was engineered based on structural analysis. Homology modeling of *Psp*A6PE was constructed using *Ec*A6PE (PDB: 3CT7, 58.5% sequence identity with *Psp*A6PE) as the template. Subsequently, molecular docking was performed with F6P as the ligand. As shown in Fig. S3A, the structure of *Psp*A6PE comprised a $(\beta/\alpha)_8$-barrel, and the eighth β-strand was used for binding substrate. A total of 24 residues are located at the substrate-binding pocket within 3 Å and have interactions (hydrogen bonds and van Der Waals force) with the ligand. Based on conservation analysis of above 24 residues (sequence blast of 1280 A6Pes in NCBI) (Fig. S3B), 9 residues (e.g., M10, C11, P141, Y143, S177, C178, I195, T198, and G200) with low conservatism were selected for further alanine scanning. As shown in Table S5, except variant S177A, other eight variants showed significantly different activities from wild-type *Psp*A6PE (WT). Consequently, these eight residues were subjected to site-directed saturation mutagenesis (Fig. S4), and three variants (Y143F, C178V, and T198S) with 30% higher activities than WT were

**Table 1**
Specific activity and kinetic parameters of *Psp*A6PE and variants.

| Enzymes | Specific Activity ($U \cdot mg^{-1}$) | $k_{cat}$ ($min^{-1}$) | $K_m$ (mM) | $k_{cat}/K_m$ ($min^{-1}$ $mM^{-1}$) |
|---|---|---|---|---|
| Wild type (WT) | 9.4 ± 0.1 | 78.2 ± 3.1 | 10.3 ± 1.1 | 7.6 |
| Y143F | 11.6 ± 0.5 | 77.9 ± 3.0 | 8.5 ± 1.8 | 9.1 |
| C178V | 12.3 ± 0.4 | 66.4 ± 3.3 | 8.8 ± 1.2 | 7.5 |
| T198S | 11.7 ± 0.2 | 73.3 ± 4.9 | 8.7 ± 1.6 | 8.4 |

obtained for further characterizations.

As shown in Table 1, compared with *Psp*A6PE WT, the activities of variants Y143F, C178V, and T198S increased by 23%, 30%, and 24%, respectively. Kinetic analysis showed that all variants displayed lower $K_m$ values than WT, suggesting enhanced substrate affinity. Moreover, variant Y143F enhanced its catalytic efficiency with the highest $k_{cat}/K_m$ value of 9.1 $min^{-1}$ $mM^{-1}$, which was 1.20-fold of that of WT. The performance of these three variants were evaluated in the cascade reaction. As shown in Fig. 4A, variant Y143F showed the highest yield of D-allulose (90.7%), which was 14.3% higher than that of WT.

Thermostability analysis of the *Psp*A6PE WT and best variant Y143F was also performed. As shown in Fig. 4B, compared with WT ($t_{1/2}$ = 14.6 min), the half-life of variant Y143F at 40 °C ($t_{1/2}$ = 24.4 min) increased by 67%, suggesting higher thermostability of variant Y143F. As shown in Fig. 4C, the optimum temperature of WT and variant Y143F was 40 °C. Moreover, Y143F showed 65.3% higher yield of D-allulose than WT at 60 °C, which was remarkably improved than that at 40 °C (only 14.3% higher yield by Y143F than WT) (Fig. 4C), also suggesting higher thermostability of variant Y143F. These results indicate that the thermostability of *Psp*A6PE plays a vital role in the cascade route for D-allulose synthesis.

Furthermore, the mechanism of enhanced catalytic efficiency of Y143F was analyzed based on its structure model. As shown in Fig. 5, one hydrogen bond was observed between Tyr143 and Lys42, causing Tyr143 to be far away from the ligand (F6P) in WT. However, in Y143F, the hydrogen bond between Phe143 and Lys42 disappeared, and one new hydrogen bond between Phe143 and the substrate F6P is formed. This phenomenon may contribute to the enhanced substrate affinity and catalytic efficiency of variant Y143F.

### 3.4. Construction and optimization of Module II (ATP regeneration)

In Module I, the phosphorylation of fructose by *Ca*FRK requires a large amount of expensive ATP as activation energy. To reduce the consumption of ATP, an ATP-regeneration system was constructed as Module II. Generally, ATP-regeneration system is a coupled system comprising ATP biosynthesis and ATP-consuming reactions (primarily based on phosphorylation) (Andexer & Richter, 2015). Kinases are typically used to catalyze the phosphorylation of ADP or AMP for ATP regeneration. Recently, PPK has been used for ATP regeneration because it can use low-cost inorganic polyphosphate as the phosphate donor.

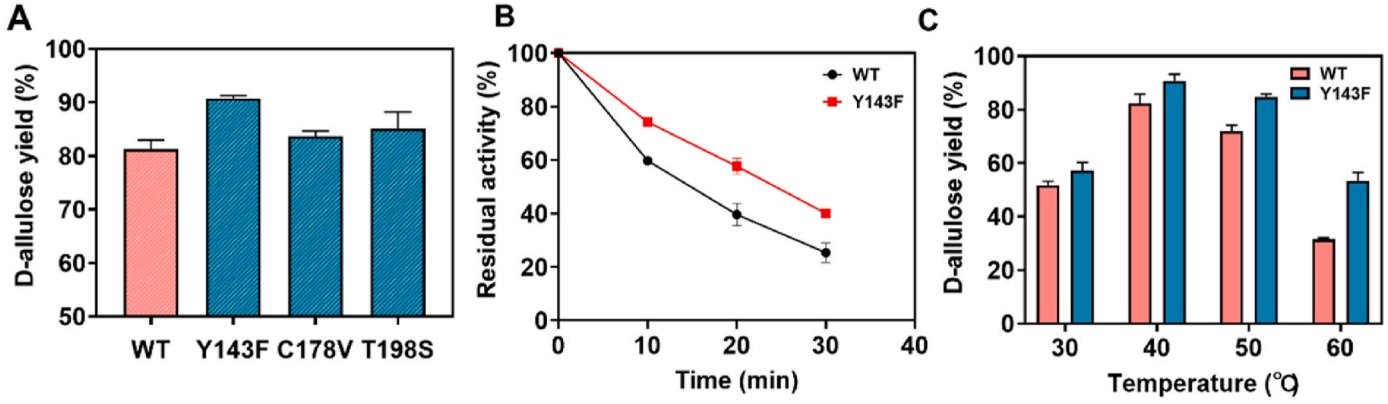


**Fig. 4.** Analysis of D-allulose yield and thermostability of *Psp*A6PE WT and variants. **(A)** Cascade synthesis of D-allulose from 10 mM fructose by *Psp*A6PE and variants. Reactions were performed using same dosage of *Psp*A6PE WT and variants (0.09 U $mL^{-1}$) for 6 h. **(B)** Thermostability of *Psp*A6PE WT and variant Y143F at 40 °C. **(C)** Cascade synthesis of D-allulose from 10 mM fructose using *Psp*A6PE WT and variant Y143F at different temperatures. Values are presented as the mean ± SD from triplicate measurements.

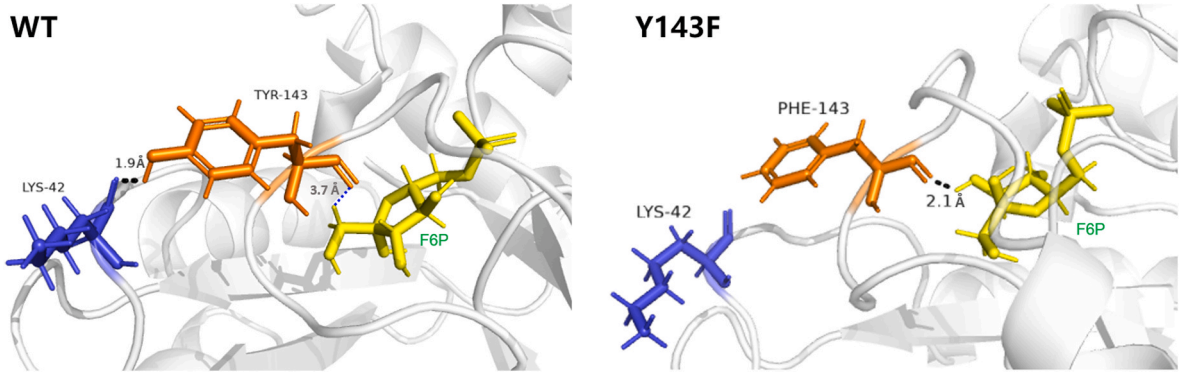


**Fig. 5.** Analysis of interactions between residues (Y143 and K42) and ligand (F6P) of *Psp*A6PE WT and variant Y143F. Hydrogen bonds are represented by dark dashed lines. The ligand is colored in yellow. (For interpretation of the references to color in this figure legend, the reader is referred to the Web version of this article.)

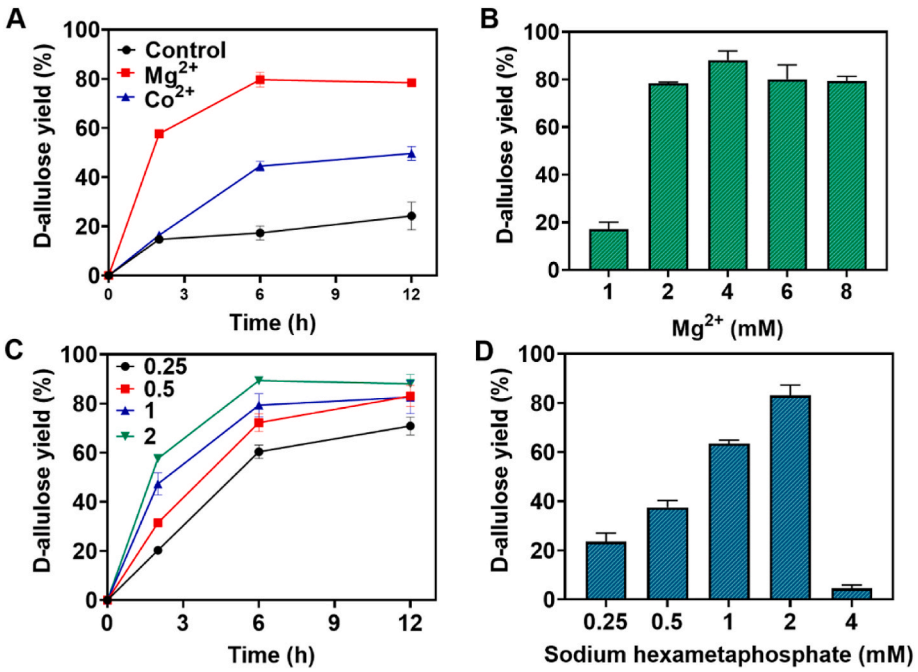


**Fig. 6.** Optimization of Module II for ATP regeneration. **(A)** Production of D-allulose from 10 mM fructose at 2 mM $Co^{2+}$ or $Mg^{2+}$. **(B)** Optimization of $Mg^{2+}$ concentration. **(C)** Optimization of ATP concentrations. **(D)** Optimization of sodium hexametaphosphate concentrations. Values are presented as the mean ± SD from triplicate measurements.

PPKs can be classified into two families based on their difference in amino acid sequence and kinetics, designated as polyphosphate kinase family 1 (PPK1) and polyphosphate kinase family 2 (PPK2) (Ishige et al., 2002; Zhang et al., 2002). Generally, the activity of PPK2 is higher than that of PPK1 when using polyphosphate as substrate to regenerate ATP. PPK2 can be divided into three subfamilies (classes I, II, and III) based on phylogenetic analysis and catalytic properties (Motomura et al., 2014). PPK2–I and PPK2-II can catalyze the generation of ATP by using ADP and AMP as the substrate, respectively. Whereas, PPK2-III can catalyze the phosphorylation of both AMP and ADP. Consequently, PPK2-III from *Deinococcus radiodurans* (*Dr*PPK) was selected for the ATP regeneration in this study.

Reactions catalyzed by PPK usually require the addition of $Mg^{2+}$, thus the effects of $Mg^{2+}$ and $Co^{2+}$ (2 mM) on PPK were investigated. With addition of $Mg^{2+}$, the yield of D-allulose was 78.2% higher than that using $Co^{2+}$ at 12 h (Fig. 6A). Subsequently, the concentration of $Mg^{2+}$ was optimized to be 4 mM (Fig. 6B). The effect of various ATP concentrations (0.25, 0.5, 1, and 2 mM) on yields of D-allulose after introducing the ATP-regeneration system was also investigated. As shown in Fig. 6C, 89.3% yield of D-allulose was obtained at 2 mM ATP, which is higher than that at 10 mM ATP without Module II (Fig. 3D). Moreover, with decreased ATP concentration to 5% of the substrate (0.5 mM), the yield of D-allulose retained over 80%, suggesting that the introduced ATP-regeneration system can efficiently reduce ATP consumption without significantly affecting the yield of D-allulose. Additionally, the effect of sodium hexametaphosphate concentration was also investigated, and the optimum concentration of sodium hexametaphosphate was determined to be 2 mM (Fig. 6D).

### 3.5. Construction and optimization of Module III (sucrose phosphorolysis)

To replace D-fructose with cheap sucrose as the substrate, Module III for sucrose phosphorolysis was constructed. Sucrose phosphorylase was introduced to catalyze the phosphorylation of sucrose for producing D-fructose, which was further converted into D-allulose by Modules I and II. Given that phosphorylation requires phosphate as a donor, PBS buffer (pH 8.0) was used instead of Tris-HCl buffer (pH 8.0).

In Module III, sucrose phosphorylases from *B. adolescentis* (*Lm*SP) and *Leuconostoc mesenteroides* (*Ba*SP) were evaluated, and their specific

**Table 2**
Summary of D-allulose produciton under different conditions.

| Sucrose (mM) | [a] Strategy | [b] Co-substrates concentration | PBS (mM) | [c] Enzymes dosage | Yield (%) | Space–time yield ($g \cdot L^{-1} \cdot h^{-1}$) | Production ($g \cdot L^{-1}$) | S/C ( × $10^3$) |
|---|---|---|---|---|---|---|---|---|
| 10 | one-pot | 1 × Init | 10 | 1 × Dos | 88.8 | 0.13 | 1.6 | 4.4 |
| 20 | one-pot | 2 × Init | 20 | 1 × Dos | 84.5 | 0.25 | 3.0 | 8.8 |
| 20 | one-pot | 2 × Init | 20 | 2 × Dos | 85.6 | 0.26 | 3.1 | 4.4 |
| 50 | one-pot | 5 × Init | 50 | 1 × Dos | 38.5 | 0.29 | 3.5 | 22 |
| 50 | one-pot | 5 × Init | 50 | 2.5 × Dos | 70.8 | 0.53 | 6.4 | 8.8 |
| 50 | one-pot | 5 × Init | 10 | 2.5 × Dos | 82.8 | 0.62 | 7.4 | 8.8 |
| 100 | one-pot | 10 × Init | 10 | 5 × Dos | 45.8 | 0.69 | 8.3 | 8.8 |
| 100 | Two-step | 10 × Init | 10 | 5 × Dos | 70.4 | 1.06 | 12.7 | 8.8 |

[a] "one-pot" means that all substrates (including co-substrates), enzymes, and PBS buffer were simultaneously added to the reaction mixture. "two-step" means the whole MCAS route comprises two steps. The first step was the phosphorylation of sucrose catalyzed by BaSP in PBS buffer (pH 8.0). After 2 h, in the second step other co-substrates (e.g., ATP and sodium hexametaphosphate) and enzymes (e.g., PspA6PE, CaFRK, CtA6PP, and DrPPK) were added to the mixture for continued reaction.
[b] "Init" means the initial concentrations of co-substrates (sodium hexametaphosphate/ATP/$Mg^{2+}$ = 2 mM/0.5 mM/4 mM).
[c] "Dos" means the initial dosage (2.25 μM) of all enzymes including *Ba*SP (0.15 μM), *Ca*FRK (0.4 μM), *Psp*A6PE (0.8 μM), *Ct*A6PP (0.4 μM), and *Dr*PPK (0.5 μM).

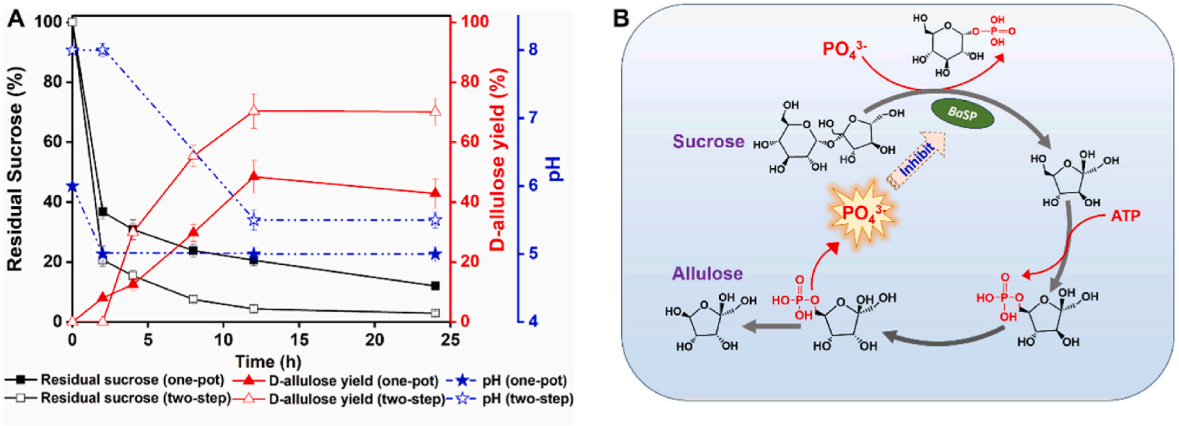


**Fig. 7.** **(A)** Time course of D-allulose yield, residual sucrose, and pH with 100 mM sucrose as substrate by one-pot and two-step strategies. The reaction was performed in a 5-mL tube containing 2 mL of mixture: 100 mM sucrose, 10 mM PBS (pH 8.0), 40 mM $MgCl_2$, 5 mM ATP, 20 mM sodium hexametaphosphate, *Ba*SP (43.9 U·mL$^{-1}$, 0.75 μM), *Ca*FRK (2.8 U·mL$^{-1}$, 2 μM), *Psp*A6PE (1.9 U·mL$^{-1}$, 4 μM), *Ct*A6PP (0.005 U·mL$^{-1}$, 2 μM), and *Dr*PPK (0.1 mg mL$^{-1}$, 2.5 μM). Incubation was conducted at 40 °C for 24 h. **(B)** Proposed regulation mechanism of phosphate on cascade biosynthesis of D-allulose.

activities of *Lm*SP and *Ba*SP were 461 and 351 U·mg$^{-1}$, respectively. Whereas, the residual activity of *Ba*SP (100%) was 4-fold of that of *Lm*SP (25%) after 30 min at 50 °C, suggesting the higher thermostability of *Ba*SP (Fig. S5A). Moreover, *Ba*SP yielded up to >90% of fructose from sucrose at 10 min at 50 °C and 60 °C, and remained stable with prolonged time, which was 6–8-fold higher than that of *Lm*SP (Fig. S5B). Thus, *Ba*SP was selected for Module III in this study.

Based on the above optimizations, the complete MCAS route including three Modules (I, II and III) was performed as follows: 10 mM PBS buffer (pH 8.0), 0.5 mM ATP, 4 mM $MgCl_2$, 2 mM sodium hexametaphosphate, 8.78 U·mL$^{-1}$ (0.15 μM) *Ba*SP, 0.56 U·mL$^{-1}$ (0.4 μM) *Ca*FRK, 0.38 U·mL$^{-1}$ (0.8 μM) *Psp*A6PE, 0.001 U·mL$^{-1}$ (0.4 μM) *Ct*A6PP, and 0.02 mg mL$^{-1}$ (0.5 μM) *Dr*PPK. Under above conditions, 88.8% D-allulose was obtained from 10 mM sucrose.

### 3.6. D-Allulose synthesis at elevated concentrations of sucrose

Elevated concentrations of sucrose were attempted in MCAS route for D-allulose synthesis. As shown in Table 2, with increased sucrose concentration to 20 mM, a marginal increasement of D-allulose yield (from 84.5% to 85.6%) when total enzymes dosage increased from 2.25 μM (S/C = $8.8 \times 10^3$) to 4.5 μM (S/C = $4.4 \times 10^3$), indicating little effect of enzymes amount for the cascade reaction at 20 mM sucrose. However, when sucrose concentration increased to 50 mM, the yield of D-allulose dramatically decreased to 38.5% with 2.25 μM of enzymes dosage (S/C = $2.2 \times 10^4$), and increased to 70.8% with increased enzyme dosage to 2.5-fold (S/C = $8.8 \times 10^3$), suggesting pivotal role of sufficient enzymes dosage at the elevated concentration (50 mM) of sucrose. Furthermore, the decreased PBS concentration (10 mM) was conducive to D-allulose production, resulting 82.8% yield at 50 mM sucrose, suggesting the phosphate concentration plays an important role in regulating the MCAS route.

However, with further increased sucrose concentration to 100 mM, the yield of D-allulose drastically decreased to 45.8% in one-pot reaction (Table 2). To understand the limitation of D-allulose production, the residual substrate (sucrose), product (D-allulose) yield, and pH were monitored during the reaction (Fig. 7A). In the one-pot strategy, all the enzymes and substrate/co-substrates were added at the beginning of the reaction. The initial pH of 6.0 was decreased to 5.0 after 2 h, then kept constant at pH 5.0 during 2–24 h. Meanwhile, nearly 40% of sucrose was remained at 2 h, and over 20% of sucrose was not utilized after 12 h. The yield of D-allulose gradually increased to 45.8% at 12 h, then slightly decreased in 12–24 h. Notably, in one-pot strategy, a substantial amount of protein precipitation was observed in the reaction, which was identified as inactivated enzymes (consistent with molecular weights of *Ba*SP, *Psp*A6PE, *Ca*FRK, and *Dr*PPK) by SDS-PAGE (Fig. S6). In the two-step strategy, the MCAS route comprised two steps. First, the phosphorylation of sucrose catalyzed by *Ba*SP was conducted in PBS buffer (pH 8.0). After 2 h, other substrates (e.g., ATP and sodium hexametaphosphate) and enzymes (e.g., *Psp*A6PE, *Ca*FRK, *Ct*A6PP, and *Dr*PPK) were added for continued reaction. During the first step (0–2 h), 80% of sucrose was utilized by *Ba*SP at pH 8.0. In the second step, D-allulose was produced and 70.4 % yield was reached with less than 5% residual sucrose at 12 h (pH 5.5) (Fig. 7A).

Using two-step MCAS strategy, the highest D-allulose yield of 70.4% was reached at an elevated sucrose of 100 mM, leading to a space-time yield of 1.06 g L$^{-1}$·h$^{-1}$ at S/C of $8.8 \times 10^3$. Compared with <30% yield in D-tagatose-3 epimerase approach (Mao et al., 2020; Wang et al., 2020), D-allulose yield of this MCAS route is over 2-fold higher. In the multi-enzyme synthesis of D-allulose from starch (Li et al., 2021), 79.2% yield was obtained by breaking thermodynamic limitation, the space-time yield (0.37 g L$^{-1}$·h$^{-1}$) was much lower than this study.

To explain the different performance of one-pot and two-step strategies, a regulatory mechanism on cascade synthesis of D-allulose was proposed (Fig. 7B). In one-pot approach, additional ATP and sodium hexametaphosphate resulted in an acidic initial pH of 6.0, which has inhibitory effect on *Ba*SP, leading to poor utilization of sucrose and $PO_4^{3-}$ (from PBS buffer). Along the reaction, most $PO_4^{3-}$ produced via dephosphorylation by A6PP was accumulated, causing a lower pH of 5.0, which further inhibited the activities of most enzymes (e.g., *Ba*SP, *Psp*A6PE, *Ca*FRK, and *Dr*PPK). In two-step strategy, sucrose phosphorylation reaction by *Ba*SP was performed under its optimum alkaline condition (pH 8.0) in the first step, and most $PO_4^{3-}$ was converted to G1P, avoiding low pH caused by excessively accumulated $PO_4^{3-}$. These results indicate that excessive $PO_4^{3-}$ is not conducive to the production of D-allulose, which may be responsible for the improved D-allulose yield from 100 mM sucrose using two-step strategy (Fig. 7A), as well as the relatively higher D-allulose yield (82.8%) in 10 mM PBS buffer at 50 mM sucrose (Table 2).

## 4. Conclusion

A novel *in vitro* cascade route (MCAS) for biosynthesis of value-added D-allulose from inexpensive sucrose was successfully constructed in *E. coli* by combining sucrose phosphorolysis (Module III), D-allulose synthesis from D-fructose (Module I), and ATP regeneration (Module II). *Psp*A6PE was further engineered by semi-rational design, and the best variant Y143F was obtained with 14.3% higher yield of D-allulose than that of WT. After optimization, 88.8% yield of D-allulose was achieved from 10 mM sucrose, and the ATP consumption was decreased to 5% of

sucrose dosage. At an elevated concentration of sucrose (100 mM), the two-step approach led to D-allulose yield of 70.4% with a space-time yield of 1.06 g $L^{-1}{\cdot}h^{-1}$ and S/C of 8.8 $\times$ $10^3$. This newly designed MCAS strategy is a potential route toward the efficient production of D-allulose with reduced cost.

## Authorship contribution statement

Ruizhi Han: Data curation, Methodology, Writing - original draft, Writing - review & editing, Project administration. Wenyu Tu: Data curation, Investigation, Writing - original draft. Shuangyu Liu: Investigation, Methodology. Yu Ji: Writing - review & editing. Ulrich Schwaneberg: Writing - review & editing. Yuanyi Guo: Methodology. Ye Ni: Writing - review & editing, Project administration, Funding acquisition, Supervision.

## Declaration of competing interest

The authors have declared that there are no conflicts of interest.

## Data availability

Data will be made available on request.

## Acknowledgments

This work was supported by the National Key Research and Development Program of China (2021YFC2102700), the National Natural Science Foundation of China (31871738, 22077054), the National First-Class Discipline Program of Light Industry Technology and Engineering (LITE2018-07), the Program of Introducing Talents of Discipline to Universities (111-2-06).

## Appendix A. Supplementary data

Supplementary data to this article can be found online at https://doi.org/10.1016/j.fbio.2023.103303.

## References

Ahmed, A., Khan, T. A., Ramdath, D. D., Kendall, C. W. C., & Sievenpiper, J. L. (2022). Rare sugars and their health effects in humans: A systematic review and narrative synthesis of the evidence from human trials. *Nutrition Reviews, 80*(2), 255–270.

Andexer, J. N., & Richter, M. (2015). Emerging enzymes for ATP regeneration in biocatalytic processes. *ChemBioChem, 16*(3), 380–386.

Andreana, P. R., McLellan, J. S., Chen, Y., & Wang, P. G. (2002). Synthesis of 2,6-dideoxysugars via ring-closing olefinic metathesis. *Organic Letters, 4*(22), 3875–3878.

Bahia, F. M., de Almeida, G. C., de Andrade, L. P., Campos, C. G., Queiroz, L. R., da Silva, R. L. V., Abdelnur, P. V., Corrêa, J. R., Bettiga, M., & Parachin, N. S. (2018). Rhamnolipids production from sucrose by engineered *Saccharomyces cerevisiae*. *Scientific Reports, 8*(1), 2905.

Chen, Y., Chen, Y., Ming, D., Zhu, L., & Jiang, L. (2023). Highly efficiency production of D-allulose from inulin using curli fiber multi-enzyme cascade catalysis. *International Journal of Biological Macromolecules, 241*, Article 124468.

Chung, M. Y., Oh, D. K., & Lee, K. W. (2012). Hypoglycemic health benefits of D-psicose. *Journal of Agricultural and Food Chemistry, 60*(4), 863–869.

Dobson, C. M. (2004). Biological physics: Energy, information, life. *Nature, 432*, 444–445.

Goedl, C., Sawangwan, T., Wildberger, P., & Nidetzky, B. (2009). Sucrose phosphorylase: A powerful transglucosylation catalyst for synthesis of α-D-glucosides as industrial fine chemicals. *Biocatalysis and Biotransformation, 28*(1), 10–21.

Gou, Y., Liu, B. Y., Cheng, M. Y., Yamada, T., Iida, T., Wang, S. X., Banno, R., & Koike, T. (2021). D-allulose ameliorates skeletal muscle insulin resistance in high-fat diet-fed rats. *Molecules, 26*(20), 6310–6321.

Han, Y. J., Kwon, E. Y., & Choi, M. S. (2020). Anti-diabetic effects of allulose in diet-induced obese mice via regulation of mRNA expression and alteration of the microbiome composition. *Nutrients, 12*(7), 2113.

Hayashi, N., Iida, T., Yamada, T., Okuma, K., Takehara, I., Yamamoto, T., Yamada, K., & Tokuda, M. (2010). Study on the postprandial blood glucose suppression effect of D-psicose in borderline diabetes and the safety of long-term ingestion by normal human subjects. *Bioscience Biotechnology & Biochemistry, 74*(3), 510–519.

Hayashi, N., Yamada, T., Takamine, S., Iida, T., Okuma, K., & Tokuda, M. (2014). Weight reducing effect and safety evaluation of rare sugar syrup by a randomized double-blind, parallel-group study in human. *Journal of Functional Foods, 11*, 152–159.

Hossain, A., Yamaguchi, F., Matsuo, T., Tsukamoto, I., Toyoda, Y., Ogawa, M., Nagata, Y., & Tokuda, M. (2015). Rare sugar D-allulose: Potential role and therapeutic monitoring in maintaining obesity and type 2 diabetes mellitus. *Pharmacology & Therapeutics, 155*, 49–59.

Iida, T., Kishimoto, Y., Yoshukawa, Y., Hayashi, N., Okuma, K., Tohi, M., Yagi, K., Matsuo, T., & Izumori, K. (2008). Acute D-psicose administration decreases the glycemic responses to an oral maltodextrin tolerance test in normal adults. *Journal of Nutritional Science and Vitaminology, 54*(6), 511–514.

Ishige, K., Zhang, H., & Kornberg, A. (2002). Polyphosphate kinase (PPK2), a potent, polyphosphate-driven generator of GTP. *Proceedings of the National Academy of Sciences, 99*, 16684–16688.

Itoh, H., Okaya, H., Khan, A. R., Tajima, S., Hayakawa, S., & Izumori, K. (1994). Purification and characterization of D-tagatose 3-epimerase from Pseudomonas sp. ST-24. *Bioscience Biotechnology & Biochemistry, 58*(12), 2168–2171.

Jiang, W., & Fang, B. (2016). Construction and evaluation of a novel bifunctional phenylalanine–formate dehydrogenase fusion protein for bienzyme system with cofactor regeneration. *Journal of Industrial Microbiology & Biotechnology, 43*(5), 577–584.

Ji, Y., Liu, J., Wang, C., Zhang, F., Xu, X., & Zhu, L. (2023). Stability improvement of aerobic granular sludge (AGS) based on Gibbs free energy change (ΔG) of sludge-water interface. *Water Research, 240*, Article 120059.

Kim, N. H., Kim, H. J., Kang, D. I., Jeong, K. W., Lee, J. K., Kim, Y., & Oh, D. K. (2008). Conversion shift of D-fructose to D-psicose for enzyme-catalyzed epimerization by addition of borate. *Applied and Environmental Microbiology, 74*(10), 3008–3013.

Kimura, T., Kanasaki, A., Hayashi, N., Yamada, T., Iida, T., Nagata, Y., & Okuma, K. (2017). D-Allulose enhances postprandial fat oxidation in healthy humans. *Nutrition, 43–44*, 16–20.

Kitaoka, M., Sasaki, T., & Taniguchi, H. (1992). Conversion of sucrose into cellobiose using sucrose phosphorylase, xylose isomerase and cellobiose phosphorylase. *Denpun Kagaku, 39*(4), 281–283.

Lim, B. C., Kim, H. J., & Oh, D. K. (2009). A stable immobilized d-psicose 3-epimerase for the production of d-psicose in the presence of borate. *Process Biochemistry, 44*(8), 822–828.

Li, Y., Shi, T., Han, P., & You, C. (2021). Thermodynamics-driven production of value-added d-Allulose from inexpensive starch by an in vitro enzymatic synthetic biosystem. *ACS Catalysis, 11*(9), 5088–5099.

Mao, S., Cheng, X., Zhu, Z., Chen, Y., Li, C., Zhu, M., Liu, X., Lu, F., & Qin, H. M. (2020). Engineering a thermostable version of D-allulose 3-epimerase from Rhodopirellula baltica via site-directed mutagenesis based on B-factors analysis. *Enzyme and Microbial Technology, 132*, Article 109441.

Mijailovic, N., Nesler, A., Perazzolli, M., Barka, E. A., & Aziz, A. (2021). Rare sugars: Recent advances and their potential role in sustainable crop protection. *Molecules, 26*(6), 1720–1740.

Mooradian, A. D. (2019). In search for an alternative to sugar to reduce obesity. *International Journal for Vitamin and Nutrition Research, 89*(3–4), 113–117.

Mooradian, A. D., Haas, M. J., Onstead-Haas, L., Tani, Y., & Tokuda, M. (2019). Naturally occurring rare sugars are free radical scavengers and can ameliorate endoplasmic reticulum stress. *International Journal for Vitamin and Nutrition Research, 90*(3–4), 1–11.

Mooradian, A. D., Smith, M., & Tokuda, M. (2017). The role of artificial and natural sweeteners in reducing the consumption of table sugar: A narrative review. *Clinical Nutrition Espen, 18*, 1–8.

Motomura, K., Hirota, R., Okada, M., Ikeda, T., Ishida, T., & Kuroda, A. (2014). A new subfamily of polyphosphate kinase 2 (class III PPK2) catalyzes both nucleoside monophosphate phosphorylation and nucleoside diphosphate phosphorylation. *Applied and Environmental Microbiology, 80*(8), 2602–2608.

Murao, K., Xiao, Y., Wen, M. C., Imachi, H., Ke, C., Muraoka, T., Kitanaka, N., Li, J., Ahmed, R., & Matsumoto, K. (2007). D-Psicose inhibits the expression of MCP-1 induced by high-glucose stimulation in HUVECs. *Life Sciences, 81*(7), 592–599.

Natsume, Y., Yamada, T., Iida, T., Ozaki, N., Gou, Y., Oshida, Y., & Koike, T. (2021). Investigation of D-allulose effects on high-sucrose diet-induced insulin resistance via hyperinsulinemic-euglycemic clamps in rats. *Heliyon, 7*(9), 1-6.

Northrup, A. B., & MacMillan, D. W. C. (2004). Two-step synthesis of carbohydrates by selective aldol reactions. *Science, 305*(5691), 1752–1755.

O'Charoen, S., Hayakawa, S., & Ogawa, M. (2015). Food properties of egg white protein modified by rare ketohexoses through Maillard reaction. *International Journal of Food Science and Technology, 50*(1), 194–202.

Qi, X., & Tester, R. F. (2020). Lactose, maltose, and sucrose in health and disease. *Molecular Nutrition & Food Research, 64*(8), Article e1901082.

Saheki, S., Takeda, A., & Shimazu, T. (1985). Assay of inorganic phosphate in the mild pH range, suitable for measurement of glycogen phosphorylase activity. *Analytical Biochemistry, 148*, 4.

Suna, S., Yamaguchi, F., Kimura, S., Tokuda, M., & Jitsunari, F. (2007). Preventive effect of D-psicose, one of rare ketohexoses, on di-(2-ethylhexyl) phthalate (DEHP)-induced testicular injury in rat. *Toxicology Letters, 173*(2), 107–117.

Takata, M., Yamaguchi, F., Nakanose, K., Watanabe, Y., Hatano, N., Tsukamoto, I., Nagata, M., Izumori, K., & Tokuda, M. (2005). Neuroprotective effect of D-psicose on 6-hydroxydopamine-induced apoptosis in rat pheochromocytoma (PC12) cells. *Journal of Bioscience and Bioengineering, 100*(6), 511–516.

Tatsuhiro, M., Hiroo, S., Mineo, H., & Ken, I. (2002). D-psicose is a rare sugar that provides no energy to growing rats. *Journal of Nutritional Science and Vitaminology, 48*(1), 77–80.

Van Laar, A. D. E., Grootaert, C., & Van Camp, J. (2021). Rare mono- and disaccharides as healthy alternative for traditional sugars and sweeteners? *Critical Reviews in Food Science and Nutrition, 61*(5), 713–741.

Wang, Y., Ravikumar, Y., Zhang, G., Yun, J., Zhang, Y., Parvez, A., Qi, X., & Sun, W. (2020). Biocatalytic synthesis of D-Allulose using novel D-tagatose 3-epimerase from christensenella minuta. *Frontiers of Chemistry, 8*, Article 622325.

Wang, M., Wu, J., & Wu, D. (2018). Cloning and expression of the sucrose phosphorylase gene in Bacillus subtilis and synthesis of kojibiose using the recombinant enzyme. *Microbial Cell Factories, 17*(1), 23–31.

Xu, J. Z., Ruan, H. Z., Yu, H. B., Liu, L. M., & Zhang, W. (2020). Metabolic engineering of carbohydrate metabolism systems in Corynebacterium glutamicum for improving the efficiency of L-lysine production from mixed sugar. *Microbial Cell Factories, 19*(1), 39.

Zhang, H., Ishige, K., & Kornberg, A. (2002). A polyphosphate kinase (PPK2) widely conserved in bacteria. *Proceedings of the National Academy of Sciences, 99*, 16678–16683.

Zhu, P., Zeng, Y., Chen, P., Men, Y., Yang, J., Yue, X., Zhang, J., Zhu, Y., & Sun, Y. (2020). A one-pot two-enzyme system on the production of high value-added D-allulose from Jerusalem artichoke tubers. *Process Biochemistry, 88*, 90–96.